INVERSE DISCONTINUITY FORMULATION OF FRACTURE

M. Fagerström[1] and R. Larsson[1]
[1] Department of Applied Mechanics, Chalmers University of Technology, Göteborg, Sweden

ABSTRACT

A theoretical and computational framework for linear and non-linear fracture mechanics is presented. We use the material forces concept as a basis for the formulation, due to the close relation between on one hand the Eshelby energy-momentum tensor and on the other hand material defects like cracks and material inhomogeneities. By separating the discontinuous displacement from the continuous counterpart in line with the eXtended Finite Element Method (XFEM), we are able to formulate the weak equilibrium in two coupled problems representing the total deformation. However, in contrast to standard XFEM, where the direct motion discontinuity is used to model the crack, we rather formulate an inverse motion discontinuity to model crack development. The resulting formulation thus couples the continuous direct motion to the inverse discontinuous motion, which may used to simulate linear as well as nonlinear fracture in one and the same formulation. In fact, the linear fracture formulation can be retrieved from the non-linear cohesive zone formulation simply by confining the cohesive zone to the crack tip.

1 INTRODUCTION

The material forces concept, originating from the work by Eshelby in the beginning of the fifties, is often used within fracture mechanical modelling due to the close connection between these forces and material inhomogeneities and discontinuities, see for instance Maugin [1], Gurtin [2], Steinmann [3] and Steinmann et al. [4].

The objective of this work is to establish a theoretical and computational framework for fracture modelling unifying linear (LEFM) and non-linear (NLFM) fracture behaviour on the basis of the inverse deformation problem with an applied discontinuous deformation separated from continuous deformation using the so-called eXtended Finite Element Method (XFEM), originally introduced by Belytschko and Black [5] or perhaps rather the partitions of unity concept for crack propagation suggested by Wells and Sluys [6]. As a result we obtain a unifying Lagrangian/Eulerian description of the fracture mechanical problem. A strong discontinuity formulation of the crack kinematics is thereby exploited for both the direct and the inverse deformation maps, leading to unique push-forward - pull-back transformations between the material and spatial discontinuities. Moreover, upon introducing the material (Eshelby) stress a separation of the continuous direct motion and the discontinuous inverse motion problems is obtained in the weak form of the momentum balance. Thereby, the solution of the continuous forward and the discontinuous inverse problems may be formulated as a coupled problem between the direct continuous deformation map and the inverse (material) discontinuity. Interesting features of the present formulation is that, firstly, a cohesive fracture mechanical model is formulated in the inverse material (crack closing) discontinuity evolution, rather than in the direct spatial (crack opening) discontinuity evolution. Secondly, the classical notion of LEFM may be distinguished from NLFM simply in terms of the extension of the cohesive zone.

2 KINEMATICS

In this section we discuss the kinematical representation of the crack. Subsection 2.1 covers the direct motion description and in the subsequent subsection we consider the inverse motion and also define the inverse discontinuity and the relation between the same and the direct counterpart.

2.1 Direct discontinuity

As a basis for the kinematical description we first consider the direct deformation map which maps points in the material reference configuration, $\boldsymbol{X} \in B_0$, onto points in the deformed spatial configuration, $\boldsymbol{x} \in B$ as

$$\boldsymbol{\varphi}\left[\boldsymbol{X},t\right] = \boldsymbol{\varphi}_c\left[\boldsymbol{X},t\right] + H_S\left[S\left[\boldsymbol{X}\right]\right]\boldsymbol{d}\left[\boldsymbol{X},t\right] \text{ with } \boldsymbol{d} = \boldsymbol{x} - \boldsymbol{x}_c \tag{1}$$

where $H_S\left[S\left[\boldsymbol{X}\right]\right]$ is the Heaviside function centered at the internal (closed) discontinuity boundary, Γ_S, shown in Figure 1. The argument $S\left[\boldsymbol{X}\right]$ is defined as

$$S\left[\boldsymbol{X}\right] < 0 \;\; \boldsymbol{X} \in D_0^-,\; S\left[\boldsymbol{X}\right] = 0 \;\; \boldsymbol{X} \in \Gamma_S,\; S\left[\boldsymbol{X}\right] > 0 \;\; \boldsymbol{X} \in D_0^+ \tag{2}$$

with the additional requirement

$$\boldsymbol{N} = \frac{\partial S\left[\boldsymbol{X}\right]}{\partial \boldsymbol{X}} \text{ with } \left|\frac{\partial S\left[\boldsymbol{X}\right]}{\partial \boldsymbol{X}}\right| = 1 \text{ for } \boldsymbol{X} \in \Gamma_S \tag{3}$$

where $\boldsymbol{N}$ is the normal vector to Γ_S pointing into the region D_0^+. Note that the total deformation map consist of one continuous part, $\boldsymbol{\varphi}_c$, defined on B_0 and a discontinuous part, $\boldsymbol{d}$, defined on a subregion D_0 of B_0 (grey area) with assumed Dirichlet boundary conditions along the boundary $\partial D_0^+ \backslash \Gamma_S$.

The pertinent deformation gradient becomes

$$\boldsymbol{F} = \boldsymbol{\varphi} \otimes \boldsymbol{\nabla}_X = \boldsymbol{F}_c + H_S \boldsymbol{F}_d + \delta_S\, \boldsymbol{d} \otimes \boldsymbol{N} \tag{4}$$

with

$$\boldsymbol{F}_c = \boldsymbol{\varphi}_c \otimes \boldsymbol{\nabla}_X \text{ and } \boldsymbol{F}_d = \boldsymbol{d} \otimes \boldsymbol{\nabla}_X \tag{5}$$

where $\delta_S[S[\boldsymbol{X}]]$ is the Dirac delta function.

2.1 Inverse discontinuity

With the kinematical representation above it is straightforward to formulate the equilibrium in the weak sense, as done in e.g. Wells et al. [7]. However, since we want to introduce the Eshelby energy-momentum tensor we further extend the kinematical framework to also include an inverse discontinuity.

First, we consider a material point on the internal discontinuity boundary Γ_S which due to separation of the material is defined in two inverse deformation maps mapping the corresponding points on either side of the crack in the spatial configuration back to the single point in the reference configuration, as shown in the right part of Figure 1. Thus we have

$$\boldsymbol{X} = \boldsymbol{\phi}_c[\boldsymbol{x}_c, t] = \boldsymbol{\phi}[\boldsymbol{x}, t] \tag{6}$$

with

$$\boldsymbol{\phi}_c[\boldsymbol{x}_c, t] = \boldsymbol{\varphi}_c^{-1} \text{ and } \boldsymbol{\phi}[\boldsymbol{x}, t] = \boldsymbol{\varphi}^{-1} \tag{7}$$

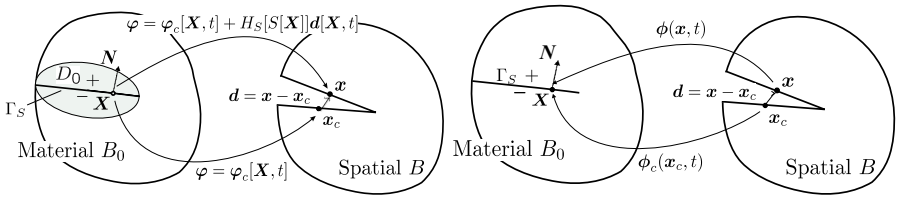

Figure 1: Kinematical representation of the discontinuous direct (left) and inverse (right) motion problem.

By differentiation eqn (6) with respect to time and introducing the direct velocities, $\boldsymbol{v}_c = \dot{\boldsymbol{\varphi}}_c$ and $\boldsymbol{v} = \boldsymbol{v}_c + \dot{\boldsymbol{d}}$, we obtain

$$\dot{\boldsymbol{X}} = \boldsymbol{f}_c \cdot \boldsymbol{v}_c + \boldsymbol{V}_c = \boldsymbol{0} \tag{8}$$

$$\dot{\boldsymbol{X}} = \boldsymbol{f} \cdot (\dot{\boldsymbol{\varphi}}_c + H_S \dot{\boldsymbol{d}}) + \boldsymbol{V} = \boldsymbol{0} \tag{9}$$

with $\boldsymbol{f}_c$ and $\boldsymbol{f}$ being the continuous and total inverse deformation gradient respectively and where

$$\boldsymbol{V}_c = \frac{\partial \boldsymbol{\phi}_c[\boldsymbol{x}_c, t]}{\partial t} \text{ and } \boldsymbol{V} = \frac{\partial \boldsymbol{\phi}[\boldsymbol{x}, t]}{\partial t} \tag{10}$$

We define the inverse discontinuity in terms of its time derivative with respect to fix spatial configuration $\overset{\circ}{\boldsymbol{D}} = \left.\dfrac{\partial \boldsymbol{D}}{\partial t}\right|_{\boldsymbol{x} \text{ fixed}}$ as

$$\overset{\circ}{\boldsymbol{D}} = \boldsymbol{V} - \boldsymbol{V}_c \tag{11}$$

By using eqns (8) and (9) we may express the relation between the direct and inverse discontinuity as

$$H_S \; \boldsymbol{f} \cdot \dot{\boldsymbol{d}} = -[\![\boldsymbol{f}]\!] \cdot \boldsymbol{v}_c - \overset{\circ}{\boldsymbol{D}} \tag{12}$$

where $[\![\boldsymbol{f}]\!] = \boldsymbol{f} - \boldsymbol{f}_c$. The relation may also be written in variational form as

$$H_S \boldsymbol{f} \cdot \Delta \boldsymbol{d} = -[\![\boldsymbol{f}]\!] \cdot \Delta \boldsymbol{\varphi}_c - \delta \boldsymbol{D} \tag{13}$$

where Δ denotes variations with respect to the reference configuration and δ variations with respect to spatial configuration.

3 WEAK FORM EQUILIBRIUM

Using the classical formulation of the weak form equilibrium in terms of the first Piola-Kirchhoff stress tensor, $\boldsymbol{\Sigma}_1^t$, and possible body forces, $\boldsymbol{b}^{mec}$, along with the kinematics described in Subsection 2.1 considering the continuous portion, $\boldsymbol{\varphi}_c$ and the discontinuity, $\boldsymbol{d}$, as two independent fields enables one to formulate the equilibrium in two coupled equations, one continuous and one discontinuous as done in e.g Wells et al. [7]. It is rather straightforward to introduce finite element discretizations for $\boldsymbol{\varphi}_c$ and $\boldsymbol{d}$ which superimposed give the total deformation. However, as earlier mentioned we are interested in including the energy-momentum tensor, $\boldsymbol{M}^t = \rho_0 \psi \boldsymbol{1} - \boldsymbol{T}$ (with $\boldsymbol{T}$ being the material mandel stress tensor and ψ being Helmholtz free energy per unit of volume), why we also include the inverse discontinuity in view of eqn (13) which (after some derivations) leads to two coupled equilibrium equations. One for the direct continuous displacement and one for the inverse discontinuous displacement as

$$(C): \quad \int_{V_0} \boldsymbol{\Sigma}_1^t : \Delta \boldsymbol{F}_c \, dV = \int_{\Gamma_0} \Delta \boldsymbol{\varphi}_c \cdot \boldsymbol{t}_1 d\Gamma + \int_{V_0} \Delta \boldsymbol{\varphi}_c \cdot \boldsymbol{b}^{mec} dV \tag{14}$$

$$(D): \quad \begin{aligned} &\int_{D_0} H_S \boldsymbol{M}^t : \delta \boldsymbol{L}_D \; dV + \int_{\Gamma_S} \delta \boldsymbol{D} \cdot \boldsymbol{M}^t \cdot \boldsymbol{N} d\Gamma = \\ &\int_{D_0} H_S \, \delta \boldsymbol{D} \cdot (\boldsymbol{B}^{mec} + \boldsymbol{B}^{inh}) \; dV \end{aligned} \tag{15}$$

Here we have introduced the first Piola-Kirchhoff traction vector, $\boldsymbol{t}_1 = \boldsymbol{\Sigma}_1^t \cdot \boldsymbol{N}$, the discontinuous inverse velocity gradient, $\delta \boldsymbol{L}_D = \delta \boldsymbol{D} \otimes \boldsymbol{\nabla}_X$, the material body force, $\boldsymbol{B}^{mec} = -\boldsymbol{F}^t \cdot \boldsymbol{b}^{mec}$, and the material inhomogeneity force, $\boldsymbol{B}^{inh} = -\left.\dfrac{\partial(\rho_0 \psi)}{\partial \boldsymbol{X}}\right|_{expl}$, i.e. the explicit dependency of $(\rho_0 \psi)$ on $\boldsymbol{X}$. Note that the normal vector $\boldsymbol{N}$ is pointing from the minus to the plus side of the interface, and that Dirichlet boundary conditions are assumed along $\partial D_0^+ \backslash \Gamma_S$ for $\boldsymbol{D}$.

In the non-linear case we allow for a successive degradation of the stresses along Γ_S using a cohesive zone formulation whereas in the linear case the cohesive zone is confined to the crack tip rendering the vectorial form of the J-integral as a reaction force at the crack tip.

4.1 Linear fracture

In the linear case we subdivide the internal boundary in one regular and one singular part recognizing the fact that the physical stresses are zero on the regular part of Γ_S which leads to

$$\begin{aligned}\int_{\Gamma_S} \delta\boldsymbol{D}\cdot\boldsymbol{M}^t\cdot\boldsymbol{N}d\Gamma_S &= \int_{\Gamma_{S^r}} \rho_0\,\psi\,\delta\boldsymbol{D}\cdot\boldsymbol{N}d\Gamma_S + \int_{\Gamma_{S^s}} \delta\boldsymbol{D}\cdot\boldsymbol{M}^t\cdot\boldsymbol{N}^s d\Gamma_S = \\ &= \int_{\Gamma_{S^r}} \rho_0\,\psi\,\delta\boldsymbol{D}\cdot\boldsymbol{N}d\Gamma_S - \delta\boldsymbol{A}\cdot\boldsymbol{J}\end{aligned} \tag{16}$$

where we included also the crack tip extension $\delta\boldsymbol{A}$ defined as $\delta\boldsymbol{A} = -\delta\boldsymbol{D}(\boldsymbol{X}_A)$, even though we have a Dirichlet boundary condition at the crack tip and where $\boldsymbol{N}^s$ is the non-unique normal vector at the singular point of the discontinuity surface. It appears that the corresponding force variable $\boldsymbol{J}$ to $\delta\boldsymbol{A}$ is the vectorial form of the J-integral, first introduced by Rice [8]. Evidently, the J-integral is obtained as a reaction force at the crack tip due to the material discontinuity development. Therefore, the computation thereof follows the basic steps of reaction force calculation, i.e. introduce a local interpolation for the kinematic variable associated with the reaction force and evaluate the reaction force from the principle of virtual work. We thus consider the local interpolation

$$\delta\boldsymbol{D} = -N[\boldsymbol{X}]\,\delta\boldsymbol{A} \Rightarrow \delta\boldsymbol{D}\otimes\boldsymbol{\nabla}_X = -\delta\boldsymbol{A}\otimes\boldsymbol{G} \text{ with } \boldsymbol{G} = \frac{\partial N[\boldsymbol{X}]}{\partial\boldsymbol{X}} \tag{17}$$

where $N[\boldsymbol{X}]$ is an interpolation function with local support D_{0l} in the vicinity of the crack tip, as shown in Figure 2.

Upon inserting eqn (17) into eqn (16) and using the fact that the normal vector $\boldsymbol{N}^s$ is non-unique, the Heaviside function H_S can be removed within the integrands, and the crack driving force is obtained as

$$\boldsymbol{J} = \int_{D_{0l}} \Big(N[\boldsymbol{X}](\boldsymbol{B}^{mec}+\boldsymbol{B}^{inh}) - \boldsymbol{M}^t\cdot\boldsymbol{G}\Big)\,dV - \int_{\Gamma_{Sl^r}} \rho_0\,\psi\,N[\boldsymbol{X}]\,\boldsymbol{N}d\Gamma \tag{18}$$

Pertinent to a mode I discontinuity at the crack tip, the fracture criterion of Griffith's states that a free crack surface has been created whenever the stored elastic energy at the crack tip becomes equal to the fracture energy, i.e.

$$J = G_f^I \text{ with } J = |\boldsymbol{J}| \tag{19}$$

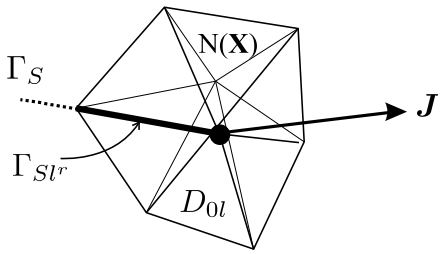

Figure 2: Local interpolation function around crack tip, for evaluation of reactive crack driving force.

where G_f^I is the fracture energy (or energy release rate) with respect to the formation of a fracture surface in mode I.

4.2 Non-linear fracture

The non-linear fracture process is considered as an isotropic damage-plasticity process and we propose a constitutive relation formulated in the crack closing traction $\boldsymbol{Q}$, as a function of the inverse discontinuity $\boldsymbol{D}$. We introduce a scalar damage variable $0 \leq \alpha \leq 1$ so that $\alpha = 0$ defines the virgin material and $\alpha = 1$ defines the completely damaged material. The traction $\boldsymbol{Q}$ is then defined in terms of α and an effective traction vector $\hat{\boldsymbol{Q}}$ as

$$\boldsymbol{Q} = (1-\alpha)\hat{\boldsymbol{Q}} \text{ with } \hat{\boldsymbol{Q}} = \boldsymbol{K} \cdot \boldsymbol{D}^e = \boldsymbol{K} \cdot (\boldsymbol{D} - \boldsymbol{D}^p) \tag{20}$$

where $\boldsymbol{D}$ is the total inverse discontinuity and $\boldsymbol{D}^p$ is the part associated with the energy dissipation. For simplicity we may chose $\boldsymbol{K}$ in terms of a scalar K, an artificial stiffness of the interface, i.e. $\boldsymbol{K} = K\boldsymbol{1}$. Next we assume an evolution equation for the damage development related to a plastic multiplier λ defined so that $\overset{\circ}{\alpha} = B\overset{\circ}{\lambda}$. Moreover, the plastic multiplier is controlled by the Karush-Kuhn-Tucker conditions $F \leq 0,\ \overset{\circ}{\lambda} \geq 0,\ F\overset{\circ}{\lambda} = 0$ where $F(\boldsymbol{Q})$ is the condition for fracture loading and unloading. We also define an evolution law for $\boldsymbol{D}^p$ in terms of a fracture potential $G(\boldsymbol{Q})$, corresponding to $F(\boldsymbol{Q})$ with no dilation in compression, as

$$\overset{\circ}{\boldsymbol{D}}{}^p = \overset{\circ}{\lambda}\frac{\partial G}{\partial \boldsymbol{Q}} = \frac{\overset{\circ}{\lambda}}{1-\alpha}\frac{\partial G}{\partial \hat{\boldsymbol{Q}}} \tag{21}$$

Additionally we chose the factor B as $B = \frac{1}{S(1-\alpha)}$ which enable us to calibrate the model for mode I fracture by choosing $S = \frac{G_f^I}{\sigma_f}$ where σ_f is the failure stress in simple tension.

4 NUMERICAL EXAMPLE

As a motivation for the proposed formulation we consider a *Single Edge Notch Test* where the predictable capabilities of the linear fracture model is clarified. The specimen in Figure 3 is under plane strain constraints and loaded vertically along the upper boundary. Moreover the material is of Neo-

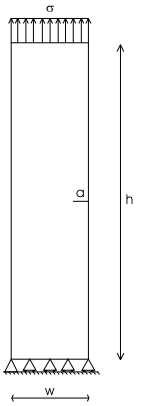

Figure 3: Hyperelastic single notch plane strain sheet loaded in tension

Hookean hyperelastic type with Helmholtz free energy defined as

$$\psi = \frac{1}{2\rho_0}\left(G\,(\mathbf{1} : (J^{-\frac{2}{3}}\,\boldsymbol{C}) - 3) + k(J-1)^2 \right) \tag{22}$$

with ρ_0 being the density of the material with respect to the reference configuration, $G = \frac{E}{2(1+\nu)}$ being the shear modulus and $k = \frac{E}{3(1-2\nu)}$ being the bulk modulus of the material and E and ν are the well known Young's modulus and Poisson's ratio respectively. Material parameters, traction magnitude and dimensions are chosen to ensure linear elastic response in order to be able to compare with analytical solutions for the J-integral using the linear elastic relation

$$J = \frac{K_I^2}{E'} \text{ with } E' = \frac{E}{1-\nu^2} \tag{23}$$

between J and K_I where K_I is the stress intensity factor for the corresponding mode I fracture case. Furthermore, the problem domain is for simplicity discretized with linear triangular finite elements, thus the same order of approximation for both $\boldsymbol{\varphi}_c$ and $\boldsymbol{D}$ is used. It turns out that the results become very sensitive to the mesh density, in particular in the vicinity of the crack tip wherefore we refine the mesh in the most sensitive region. There are no specific adaptive scheme used for the refinement but rather an intuitive step by step refinement close to the crack tip. As a result, Figure 4 shows the relative error in magnitude (left) and the angular deviation from the horizontal direction (right) of $\boldsymbol{J}$ as a function of number of elements in the analysis. Interestingly, the results imply a convergence towards the analytical value. It may also be noted that when performing a standard finite element calculation, i.e. no displacement partition, and computing $\boldsymbol{J}$ according to eqn (18) very similar results as those presented in the figure below are obtained. The maximum deviation between the results in these two analyzes is 0.2%.

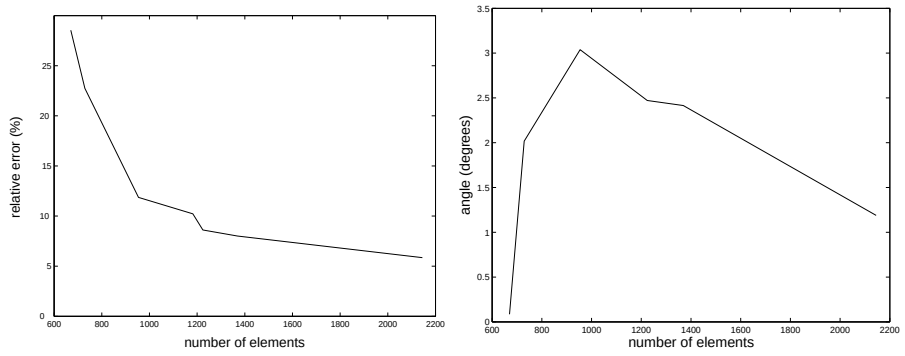

Figure 4: Reaction force convergence towards analytic value, absolute value (left) and angular deviation (right).

REFERENCES

1. G.A. Maugin. *Material Inhomogeneities in Elasticity*. Chapman & Hall, London, 1993.
2. M.E. Gurtin. *Configurational Forces as Basic Concepts of Continuum Physics*. Springer-Verlag, New York, 2000.
3. P. Steinmann. Application of material forces to hyperelastostatic fracture mechanics. I. Continuum mechanical setting. *Int. J. Solids Struct.*, 37:7371-7391, 2000.
4. P. Steinmann, D. Ackermann and F.J. Barth. Application of material forces to hyperelastostatic fracture mechanics. II. Computational setting. *Int. J. Solids Struct.*, 38:5509-5526, 2001.
5. T. Belytschko and T. Black. Elastic crack growth in finite elements with minimal remeshing. *Int. J. Numer. Meth. Engng.*, 45:601-620, 1999.
6. G.N. Wells and L.J. Sluys. A new method for modelling cohesive cracks using finite elements. *Int. J. Numer. Meth. Engng.*, 50:2667-2682, 2001.
7. G.N. Wells, R. de Borst and L.J. Sluys. A consistent geometrically non-linear approach for delamination. *Int. J. Numer. Meth. Engng.*, 54:1333-1355, 2002.
8. J.R. Rice. A path independent integral and the approximate analysis of strain concentrations by notches and cracks. *J. Appl. Mech.*, 35:397-386, 1968.